GEOPHYSICS, VOL. 63, NO. 4 (JULY-AUGUST 1998); P. 1137–1149, 10 FIGS., 1 TABLE.

Electrical conductivity of steam-flooded, clay-bearing geologic materials

David B. Butler* and Rosemary J. Knight‡

ABSTRACT

The effect of clay content on the electrical response of steamflooded geologic material is studied using a combination of laboratory experiments and numerical simulations. The presence of clay can increase the conductivity of a steam zone by providing a surface conduction path that is enhanced strongly by temperature increases. Clay also increases the residual water saturation in a steam zone, further increasing conductivity. These effects can result in steam zones that are more conductive than initial conditions. However, the presence of clay alone is not sufficient to make all portions of a steam zone conductive relative to initial conditions. Equally important to the electrical behavior is the fluid response of the reservoir to the injection of steam. In particular, the speed of the steam front, relative to the speed of the liquid water in the steam zone, plays a key role. Relatively fast-moving steam fronts cause distilled water banks to form around the front. This leads to steam zones with electrically resistive forward sections, even in clay-rich material. The rear sections of these steam zones can be either resistive or conductive, depending in part on the clay content and the salinity. Relatively slow-moving steam fronts do not cause distilled water banks to form and allow the formation of steam zones that are completely conductive relative to initial conditions.

These experimental results demonstrate the potential complexities in steam-flood electrical data. The numerical method used in this study can be used to help interpret those complexities.

INTRODUCTION

The effectiveness of steam injection for enhanced oil recovery or for ground-water remediation can be greatly increased if the progress of the steam can be monitored as it moves through the subsurface. Electrical techniques are well suited to this task because steam injection can produce large changes in subsurface conductivity. To interpret the data properly, one must understand how the physical properties of geologic material control the electrical conductivity of the steam zone. Of interest in this study is the effect of clay on the electrical response. To investigate this, we experimentally and numerically compared the electrical behavior of steam-flooded sand and clay.

Electrical conduction in clean (clay-free) sand occurs primarily by ionic conduction through the bulk pore fluid. Archie's law relates conductivity σ_b to porosity ϕ, water saturation S_w, and pore-water conductivity σ_w by (Archie, 1942)

$$\sigma_b = \phi^m S_w^n \sigma_w. \quad (1)$$

Archie found that the cementation exponent m ranges from 1.3 to 1.5 for clean, unconsolidated sands and the saturation exponent n is approximately 2.0. Steam injection affects conductivity primarily by changing S_w and σ_w, while changes in ϕ are minor and comparatively unimportant. Water saturation varies during an injection as a result of the relative movements of liquid water, oil, and steam. Pore-water conductivity depends directly upon salinity, which changes as injected water and condensed steam mix with original pore water, and upon temperature, which increases as steam moves through the material.

Laboratory studies have shown that the electrical conductivity of steam-flooded, clean sand varies in a predictable fashion as a result of these changes in temperature, salinity, and water saturation (Vaughan et al., 1993; Butler and Knight, 1995). Butler and Knight (1995) show that the steam-flood fluid response of the reservoir plays an important role in determining the shape of the conductivity profile in the reservoir. In particular, they show that a slow-moving steam front results in a

Manuscript received by the Editor May 28, 1996; revised manuscript received July 29, 1997.
*Formerly Department of Earth and Ocean Sciences, University of British Columbia, 2219 Main Mall, Vancouver, British Columbia, Canada V6T 1Z4; presently Department of Geology and Geophysics, University of Calgary, 2500 University Drive N.W., Calgary, Alberta, Canada T2N 1N4. E-mail: butler@geo.ucalgary.ca.
‡Department of Earth and Ocean Sciences, University of British Columbia. 2219 Main Mall, Vancouver, British Columbia, Canada V6T 1Z4. E-mail: knight@eos.ubc.ca.

uniform conductivity in the steam zone, but that a fast-moving steam front results in a nonuniform steam-zone conductivity. Both of these studies only used clean, initially water-saturated sands. They found that low water saturations in the steam zones dominated the electrical responses, resulting in steam zones that were more resistive than initial conditions.

However, many oil reservoirs and near-surface soils do not consist solely of clean sand and can contain appreciable amounts of clay. In contrast to the laboratory studies of clean sand mentioned earlier, field experiments in clay-bearing regions have delineated steam zones more conductive than initial conditions (Mansure et al., 1990; Newmark and Wilt, 1992; Ranganayaki et al., 1992; Ramirez et al., 1993). Clay can increase the conductivity of a reservoir by providing an additional conduction path along the clay surfaces. This surface conduction responds differently to the physical changes resulting from steam injection than does bulk-fluid conduction: it is less sensitive to water saturation and more sensitive to temperature. In addition, the presence of clays tends to increase the residual water saturation in a steam zone, thereby further increasing conductivity.

Potential factors responsible for the differences between these two sets of measurements are clay surface conduction, which is present in the field experiments and absent in the laboratory experiments; differences between the laboratory and field steam-zone water saturations, which can be related to the clay content of the materials; and differences between the steam-flood fluid responses induced in the laboratory and field injections. We assessed the importance of each factor using laboratory experiments and numerical calculations to compare the electrical conductivities of steam-flooded clean sand and clay-bearing sand.

Three aspects of this study are important to the interpretation of steam-flood monitoring data. First, steam zones in clay-rich reservoirs can become conductive relative to initial conditions as a result of enhanced clay surface conduction and high steam-zone residual water saturations. Second, this clay-rich response is overprinted by the effects of the fluid response. If the steam injection process leads to a slow-moving steam front, the reservoir becomes uniformly conductive relative to initial conditions. If a fast-moving steam front develops, the downstream, leading edge of the steam zone will be resistive while the upstream portion of the steam zone will be conductive. Third, the numerical method shown here can be used to predict the conductivity of a steam-flooded reservoir.

To understand how clay affects the electrical response, it is helpful to first review the response of a clay-free reservoir and then discuss conduction in clays. We do so briefly and follow with the results of our laboratory and numerical study of electrical conduction in clay.

THE ELECTRICAL RESPONSE OF STEAM-FLOODED SAND

One of the most important factors that determines whether a steam zone will be resistive or conductive is the ratio of conductivities of original pore water and boiler feed water. For economic reasons, produced pore water is often used as boiler feed water. Before boiling, this water is treated to remove oil, suspended solids, and dissolved oxygen and is softened by removing scaling ions such as Ca^{2+} and Mg^{2+}. However, little is done to alter the concentration of common salts such as NaCl, beyond ensuring they do not near their concentration limits (Donaldson et al., 1985). Therefore, the ratio of conductivities can be close to one. Steam generators are usually single-pass systems that boil a fraction of the incoming feed water. This fraction, referred to as *steam quality*, is typically near 80%. All of the outlet steam—part vapor (steam vapor) and part saline liquid (steam liquid)—is injected into the subsurface.

The point where steam vapor condenses defines the steam front, which marks the leading edge of the steam zone. The speed of the front depends on a number of parameters, including injection rate, steam quality, porosity, steam-zone water saturation, and heat losses to the surrounding rocks (Stewart and Udell, 1988). If one neglects heat losses, as we do in this paper, then the most important of these parameters is steam quality. Increasing the steam quality increases the heat flux into the reservoir and therefore increases the front velocity. The speed of the steam front ultimately determines what type of electrical response will occur in the reservoir.

When steam is injected into a clean, water-saturated sand, the conductivity will vary in response to the movement of heat, vapor, and salt. This situation is studied in detail by Butler and Knight (1995) and is summarized in Figure 1, showing physical and electrical changes that occur in an idealized water-saturated sand. Figure 1a comprises three sequential pictures of zones that develop during a steam flood. Figure 1b illustrates corresponding changes in temperature, saturation, salinity, and conductivity. To approximate field conditions in this example, original reservoir water and boiler feed water salinities are equal, and the injected steam has a high quality, which leads to a fast-moving steam front.

Consider t_1 in Figure 1a, a time soon after injection begins. A small steam zone has expanded outward a short distance from the injection point. Although gas and liquid coexist at the pore scale throughout the steam zone, it is instructive to split the zone into two sections based on the composition of the liquid. In the hatched area close to the injection point, the liquid is mostly injected steam liquid. This is the steam-liquid section. Injected steam vapor continuously moves through this section and moves rapidly forward to the steam front, where it condenses into distilled water. Thus, the forward part of the steam zone is the steam-condensate section, where the liquid is a mixture of condensed steam and original pore fluid. Just ahead of the steam front is a mixed zone—a fully liquid-saturated region where condensed steam vapor (distilled water) mixes with and displaces original pore fluid. Farther ahead is an undisturbed zone, where pore-fluid composition remains unchanged from initial conditions.

In Figure 1b, temperature T remains at the boiling point throughout the steam zone, then rapidly approaches the original reservoir value in the mixed zone. Water saturation S_w remains at an equilibrium level throughout much of the steam zone, then rapidly reaches 100% immediately upstream of the steam front. Ahead of the front, the sand is fully water saturated. Salinity (salt concentration c) in the steam-liquid section of the steam zone is constant. Although the boiler feed water has the same salinity as the initial pore fluid in the undisturbed zone, the steam liquid is more saline than the initial pore fluid because part of the injected water is vaporized, thus increasing the salt concentration in the liquid portion. In the steam-condensate section, salinity drops to a minimum at the steam front, where steam vapor condenses. Ahead of the steam front,

salinity again increases through the mixed zone and reaches the initial value in the undisturbed zone.

The predicted conductivity response σ at time t_1 is also shown in Figure 1b. Conductivity remains flat in the steam-liquid section and climbs slightly toward the steam front in the steam-condensate zone, a result of saturation effects overwhelming salinity effects. At this early time, temperature effects dominate in the mixed zone, and the conductivity drops slightly in the downstream direction.

At t_2 in Figure 1a, the steam zone and mixed zone have expanded, as have the steam-liquid and steam-condensate sections. The temperature and water-saturation profiles in Figure 1b have the same form as at t_1 and have moved with the steam front. The shape of the salinity curve, however, has altered somewhat. Over time, the amount of distilled water on both sides of the steam front, as a fraction of the total liquid present, has increased. Therefore, although salinity has the same general form as at t_1, the minimum value at the steam front has decreased. The corresponding conductivity response again remains flat in the steam-liquid section; initially drops in the steam-condensate section as salinity effects dominate; increases just before the steam front as saturation effects dominate; and continues to increase ahead of the steam front as salinity effects again dominate. Temperature effects are essentially unseen.

At t_3, the physical picture of the reservoir in Figure 1a and the associated temperature and saturation profiles in Figure 1b are very similar to those at t_2. However, the continued condensation of distilled water at the steam front continues to depress the salinity in that region. As a result, the conductivity seen near the steam front continues to drop. A pronounced minimum in conductivity occurs: it travels with the steam front and widens with time.

If low-quality (<50%) steam is injected, a scenario like that in Figure 2a results. In this case, steam liquid moves more quickly than the steam front. Thus, it travels through the steam zone to the front, so the liquid throughout the steam zone has a uniform salinity. At the front, the steam liquid remixes with condensing distilled water. The resulting salinity profile is seen in Figure 2b. In the steam zone it is constant at the steam-liquid value, only slightly more saline than boiler feed waters. Then, after remixing occurs at the front, it is nearly the same as in the original pore fluid, so the salinity profile ahead of the front is very nearly constant. Temperature and saturation profiles are similar to the fast-front case. The resulting conductivity profile is flat through most of the steam zone, increases close to the steam front as water saturation increases, then decreases ahead of the front as temperature decreases. No minimum appears in the conductivity profile because no distilled water bank forms.

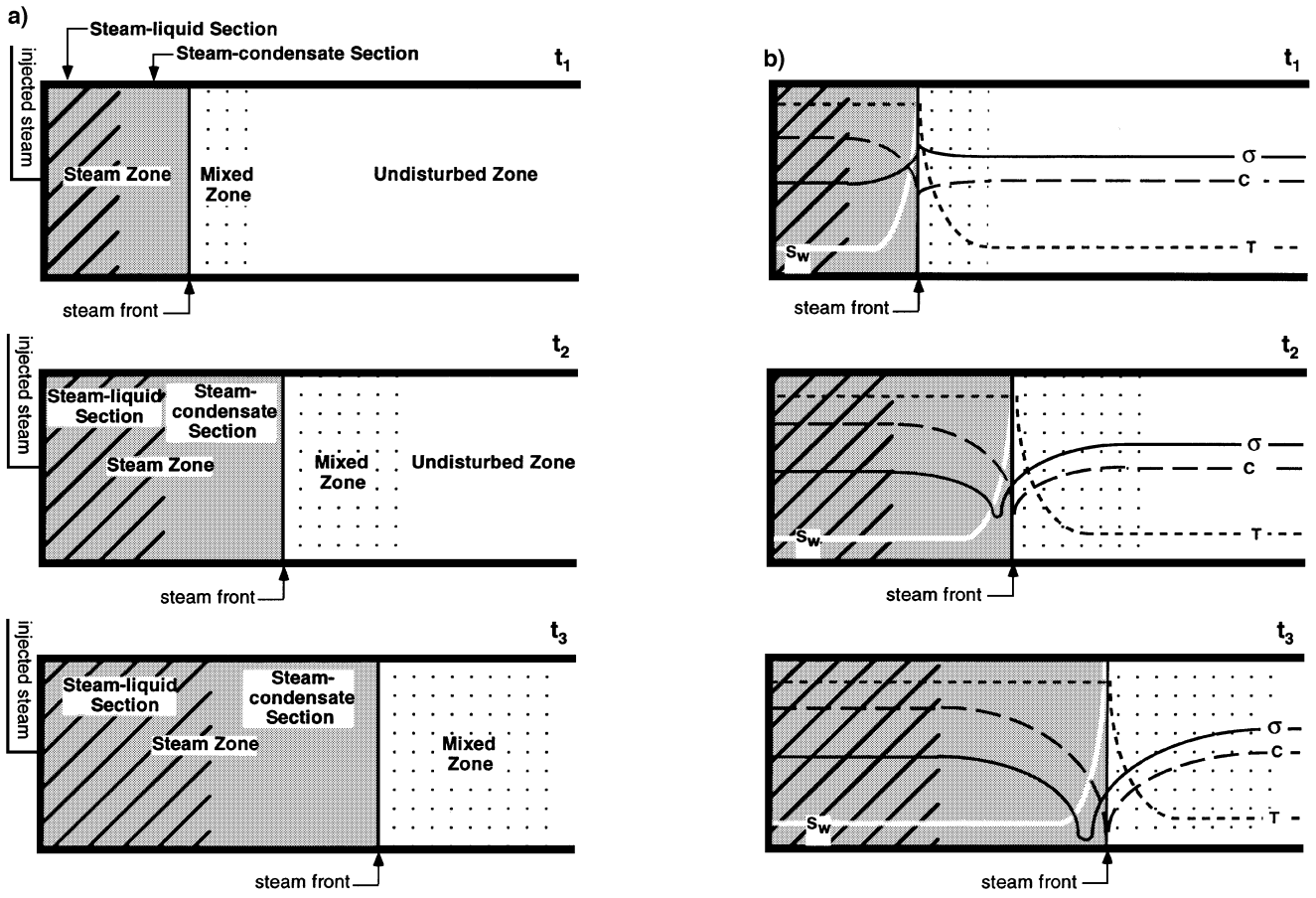

FIG. 1. (a) Affected regions in a steam-flooded reservoir and (b) associated profiles of water saturation S_w, temperature T, salinity c, and conductivity σ. These schematics are specific for the case of a fast steam front, where steam boiled from saline water is injected into a saline water-saturated reservoir.

With these explanations in mind, it becomes obvious that a number of possible conductivity responses can occur when steam is injected into clean sand. In the case where the steam front moves more slowly than the injected steam liquid and where no salinity contrast exists between original pore water and boiler feed water, the entire steam zone will be, at all times, resistive relative to initial conditions. If the boiler feed water is more saline than original pore water and the steam front moves more slowly than the injected steam liquid, then every portion of the steam zone will be conductive. However, if the steam front moves more quickly than the injected steam liquid, then regardless of feedwater salinity the development of a distilled water bank (a steam-condensate section) will temporarily dominate the electrical response, forming a conductivity minimum at the steam front. In this way the reservoir's steam-flood fluid response is a key factor in determining the electrical response.

Effects of clay on electrical response

Clay can increase the conductivity of a steam zone by providing an alternative conduction mechanism and by increasing the residual water saturation in the steam zone. The key questions we wish to address are whether this increase is sufficient to produce a conductive steam zone and whether all of the steam zone will be conductive, regardless of the steam-flood fluid response.

Clay conduction has been studied by, among others, Patnode and Wyllie (1950), Winsauer and McCardell (1953), Hill and Milburn (1956), Waxman and Smits (1968), Clavier et al. (1984), and Sen and Goode (1992). Waxman and Smits (1968) use two parameters to describe the mechanism. One is the cation concentration Q_v, a constant for a particular rock. It describes the number of cations available for conduction that are loosely attached to the negatively charged clay surface sites. The ions, which can range in concentration from zero to approximately 1.0 meq/cm^3, are in addition to those in the bulk pore fluid. The second parameter is the equivalent electrical conductance B, which describes how easily the cations can move along the clay surface. The Waxman and Smits equation (Waxman and Smits, 1968), sufficient for the purposes of this study, treats conduction as the sum of two parallel mechanisms:

$$\sigma_b = \phi^m \left(\sigma_w + \frac{BQ_v}{S_w} \right) S_w^n. \qquad (2)$$

The first term in the parentheses represents bulk pore-fluid conduction, while the second represents clay surface conduction. Clay conduction is not as strongly affected by water saturation as is conduction through the bulk pore fluid because the number of clay cations remains constant until very low levels

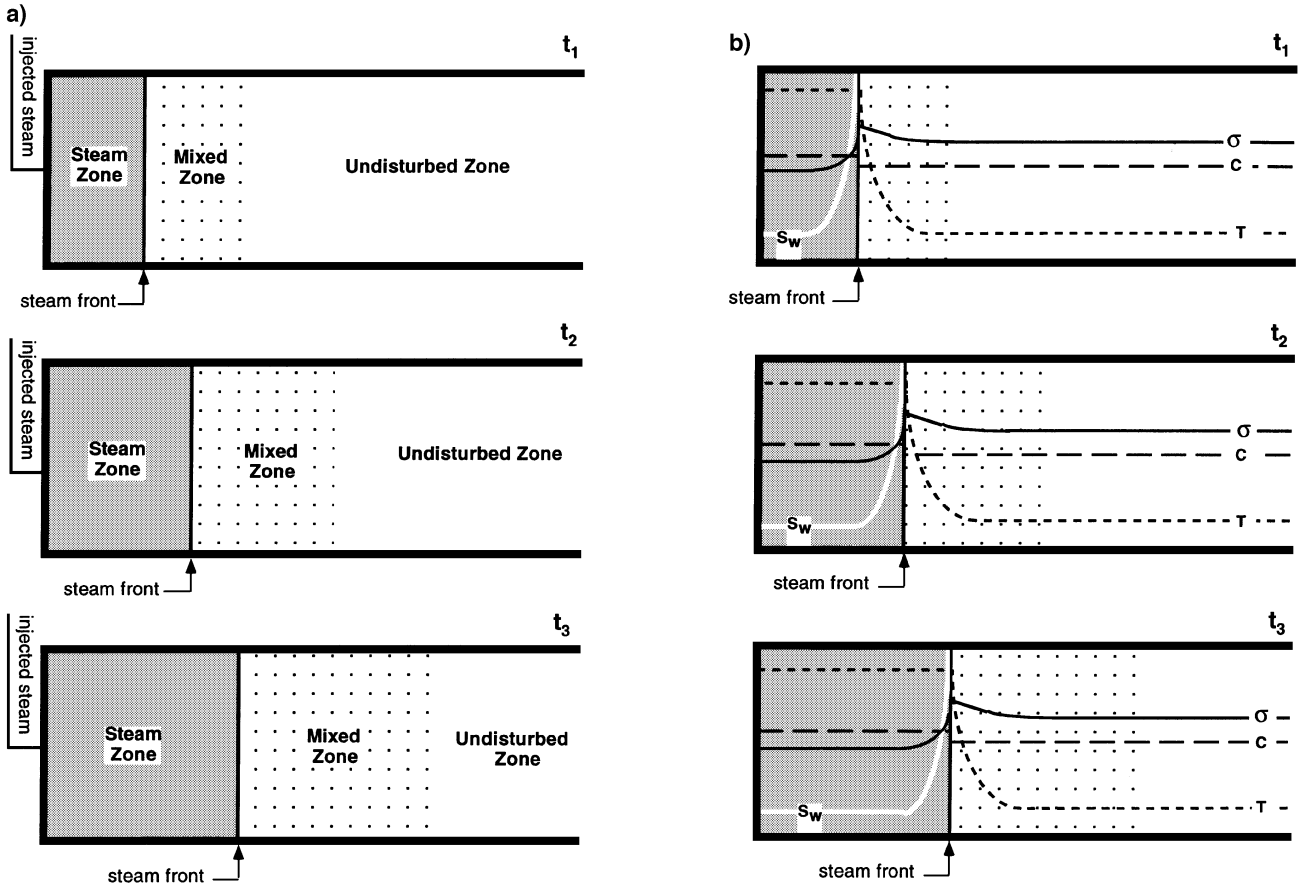

FIG. 2. (a) Affected regions in a steam-flooded reservoir and (b) associated profiles of water saturation S_w, temperature T, salinity c, and conductivity σ. These schematics are specific for the case of a slow steam front, where steam boiled from saline water is injected into a saline water-saturated reservoir.

of saturation. This is reflected by the appearance of S_w in the denominator of the clay term. Waxman and Smits (1968) observed that B depends on σ_w, increasing with pore-fluid salinity from a freshwater minimum to a saline-water maximum B_o:

$$B = B_o\left(1.0 - 0.83\exp\left(\frac{-\sigma_w}{2}\right)\right). \quad (3)$$

B_o was determined to be 3.83 Siemens per meter (S/m)/(meq/cm^3). B also depends directly on temperature (Waxman and Thomas, 1974; Sen and Goode, 1992). Mansure et al. (1990) give an approximate temperature correction that fits the data of Waxman and Thomas (1974) to within 20%:

$$B_o = 3.83(0.04T), \quad (4)$$

where T is temperature (°C). Equations (2) and (4) imply, respectively, that the presence of clay will make the conductivity of the reservoir less sensitive to saturation changes and more sensitive to temperature changes. Equations (2) and (3) together imply that clay conduction will be more important as a mechanism than bulk pore-fluid conduction at low salinities and less important at high salinities.

The residual water saturation of a reservoir, $S_{W_{irr}}$, is strongly dependent on the type and amount of clay present, and is defined as the minimum obtainable residual water saturation after the capillary displacement of water by a second immiscible fluid. Timur (1968) observed an empirical correlation between $S_{W_{irr}}$ and a reservoir's permeability k and porosity ϕ. The correlation is

$$S_{W_{irr}} = 3.5\frac{\phi^{1.26}}{k^{0.35}} - 1 \quad (5)$$

for $S_{W_{irr}}$ and ϕ in percent, and k in millidarcies. Thus compared to a clean sand, a steam-flooded, clay-bearing sand with reduced permeability is expected to have a higher steam-zone water saturation and hence a higher conductivity.

This leads us to three questions regarding steam injections into clay-bearing sands where pore water and boiler feed water have similar salinities. First, will the presence of clay be sufficient to make the steam-liquid section of a steam zone conductive relative to initial conditions? Second, if it is conductive, is that a result of clay surface conduction or increased steam-zone water saturation? Third, will the presence of clay be sufficient to make the entire steam zone conductive, regardless of the steam-flood fluid response?

To investigate in detail the effect of clay on the temporal and spatial electrical conductivity changes during a steam flood, we injected steam into clean sand and clay and compared the electrical responses. The results led us to numerically simulate injections into three other reservoirs to further delineate how clay content, permeability, and steam-front speed affect conductivity.

EXPERIMENTAL APPARATUS AND PROCEDURES

The laboratory apparatus used in this experiment is described in detail by Butler and Knight (1995). Part of the system, the electrical conductivity cell, is shown in Figure 3. It is a ceramic tube, 32.5 × 13.9 cm in diameter, filled with sand and/or clay and sealed at both ends by stainless steel plates. Steam is injected at the top of the vessel, and fluids are produced out the bottom. Small channels on the inlet and outlet faces are machined radially outward from the fluid ports. These channels, separated from the sand by wire screens, spread out the injected steam over the top and bottom of the sand. Eleven thermocouples inserted through the wall measure temperature along the tube's axis. A voltage is placed across the plates, and the electrical conductivity distribution is determined by measuring the potential differences between thermocouple sheaths. Temperatures and conductivities are measured every 2.5 s.

The approach taken in this study was to compare the steam-flood responses of clay and clean sand. Clean Ottawa sand and two clay regions were placed in the cell. The lower clay region, 90% Ottawa sand and 10% kaolinite clay, extended from just above thermocouple six (T_6 in Figure 2) to thermocouple seven (T_7). The upper region, pure kaolinite, was a 7-cm by 4-cm lens, extending from just above thermocouple three (T_3) to thermocouple four (T_4). The cell measures average conductivities between neighboring thermocouple pairs. Therefore, given the distribution of sand and clay, σ_3 and σ_6 will be most strongly

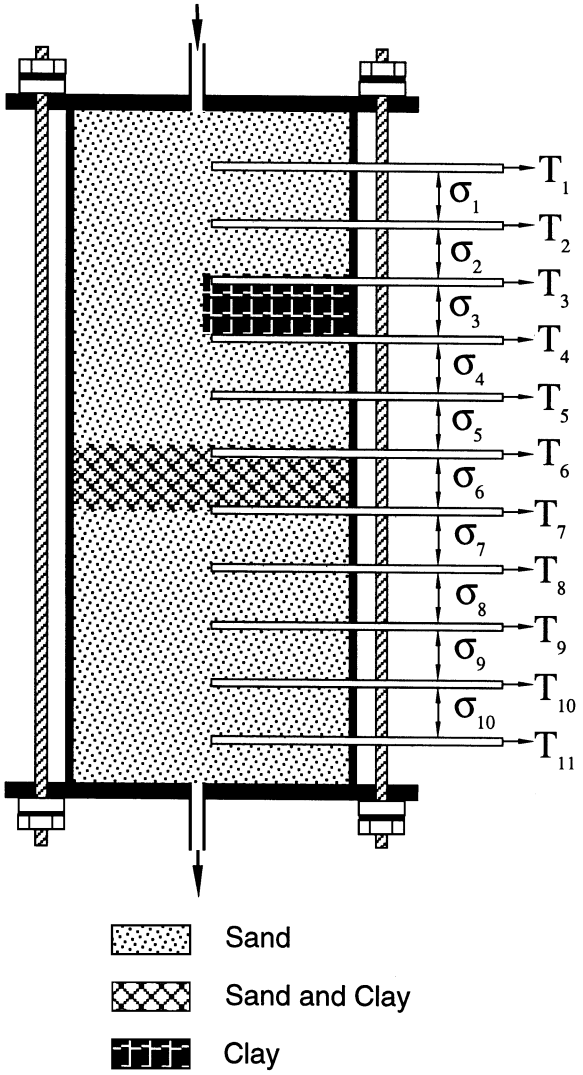

FIG. 3. Distribution of sand and clay (kaolinite) inside a conductivity cell, and the location of temperature and conductivity measurements.

affected by clay conduction; σ_2 and σ_5 may show minor clay effects; and σ_1, σ_4, σ_7, σ_8, σ_9, and σ_{10} will show only the response of clean sand.

Steam of 75% quality was chosen to match typical field values. An injection rate of 4.23 ml/minute was found to produce a stable, 1-D steam-front advance. The salinity of both the initial pore fluid and the boiler feed water was set to 0.01 M NaCl to approximate that of a freshwater oil reservoir. Monitoring of temperatures and conductivities began 10 minutes before the injection. Once steam was injected, six independently controlled heaters along the outside of the tube were used to set the external temperature distribution equal to the internal one. This was done to minimize heat losses to the outside and to help maintain a 1-D steam-front advance. Injection and monitoring continued until steam broke through the end of the cell.

EXPERIMENTAL RESULTS

Experimental data are shown in Figure 4. Temperatures, measured at specific locations as functions of time, are shown in Figure 4a. They are point measurements made along the axis of the cell at the tips of the 11 thermocouples. Each trace illustrates the data from one thermocouple. The left-hand trace, labeled T_1, corresponds to thermocouple T_1 in Figure 3; the right-hand trace, labeled T_{11}, corresponds to thermocouple T_{11}. The rest of the traces from thermocouples T_2 to T_{10} are not labeled since they follow in sequence after T_1. The temperatures, initially uniform at 25°C, increase at each point as the steam front approaches. Arrival of the front at a thermocouple is marked by the point where the temperature becomes constant. The steam-front speed varies slightly during the experiment, slowing in the clay regions. For example, the steam front takes approximately 450 s to travel through sand and clay from thermocouple T_6 to T_7, whereas it takes 300 s to travel from T_7 to T_8 in clean sand. Between 4100 and 4500 s, the temperature of the steam increases slightly from 110°C to 115°C, then decreases again to 110°C by 5200 s; this was caused by minor

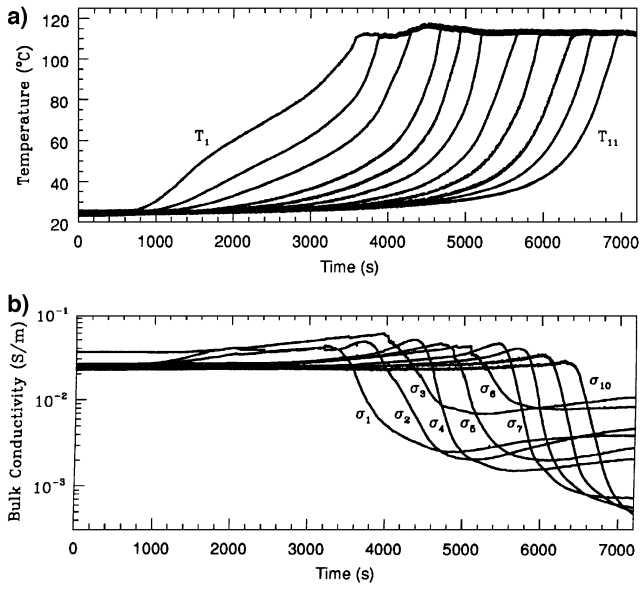

FIG. 4. Temperature (a) and electrical conductivity (b) variations with time resulting from steam injection. Curve labeling corresponds to Figure 3.

adjustments to a pressure-relief valve attached to the outlet of the cell.

Figure 4b shows the conductivity data. Again, each trace is labeled according to Figure 3; traces σ_8 and σ_9 are not labeled because of a lack of space. Most of the traces start at approximately 0.025 S/m except σ_3, which starts at 0.036 S/m. The responses can be separated into two categories: those from clean sand and those from clay.

Trace σ_1 shows a typical clean-sand response. It begins at 0.026 S/m, remains constant until 1200 s, and then gradually increases as temperatures T_1 and T_2 increase. It continues to increase with increasing temperature until 3200 s, when it reaches approximately 0.042 S/m. From the temperature data, it can be seen that steam soon arrives at the top of this conductivity-measurement region. Conductivity then decreases rapidly to 0.006 S/m at 3900 s, which as shown in Figure 4a is the time when steam reaches T_2, the thermocouple at the bottom of σ_1's measurement region. Following this, σ_1 continues to decrease at a more gradual pace, reaching a minimum conductivity of 0.0026 S/m at 4800 s. It then increases gradually and levels off at 0.004 S/m at approximately 6000 s. This pattern is repeated by all of the clean-sand regions. For example, σ_4 increases gradually as temperatures increase at T_4 and T_5 and reaches a maximum of 0.05 S/m at 4400 s, which is just before the arrival of steam at T_4. Next, it drops rapidly to 0.003 S/m at 4950 s, which is when steam reaches T_5, and then decreases more gradually to 0.0016 S/m at 5700 s. Finally, σ_4 increases slowly for the remainder of the experiment. Traces σ_7, σ_8, σ_9, and σ_{10} also follow the pattern, but the experiment was terminated while they were still decreasing. The pattern slowly evolves, as the minimum obtained conductivity decreases slowly with increasing depth in the sand. The σ_5 minimum is slightly high, but this region contains a small amount of clay at its bottom edge. The clean-sand regions also tend toward similar final conductivities, near 0.004 S/m.

The clay-sand responses are shown by σ_3 and σ_6. Trace σ_3 starts at 0.036 S/m and remains constant until 1800 s. As found for the clean-sand conductivities, it then slowly increases with increasing temperature, reaching a maximum of 0.06 S/m at 4000 s, just before the arrival of steam at T_3 at the top of the measurement region. It then decreases rapidly to 0.01 S/m at 4700 s—the point when steam reaches T_4 at the bottom of the measurement region. Next, it decreases more gradually, dropping to 0.0075 S/m by 5200 s as steam continues to move downward. Conductivity trace σ_6 behaves in a similar fashion: it increases gradually until 5100 s, slightly before the arrival of steam at T_6; decreases rapidly until 5700 s, when steam reaches T_7; decreases more slowly to 0.008 S/m at 6100 s; and then increases slightly until the end of the experiment. The major difference between these two responses and the clean-sand responses is that while both sand and clay regions have steam zones less conductive than initial conditions, the clay steam zones are more conductive than the sand steam zones.

Figure 4b displays the conductivity data as values at specific locations as functions of time. An alternative method is to view them as functions of position at specific times. Six time slices are shown in Figure 5. Each slice shows conductivity as a function of depth in the cell. The ten data correspond to the ten measurement regions of Figure 3 and are plotted at the midpoints between thermocouple locations. Hatched regions correspond to the locations of clay, and arrows show the positions of the steam front at each time.

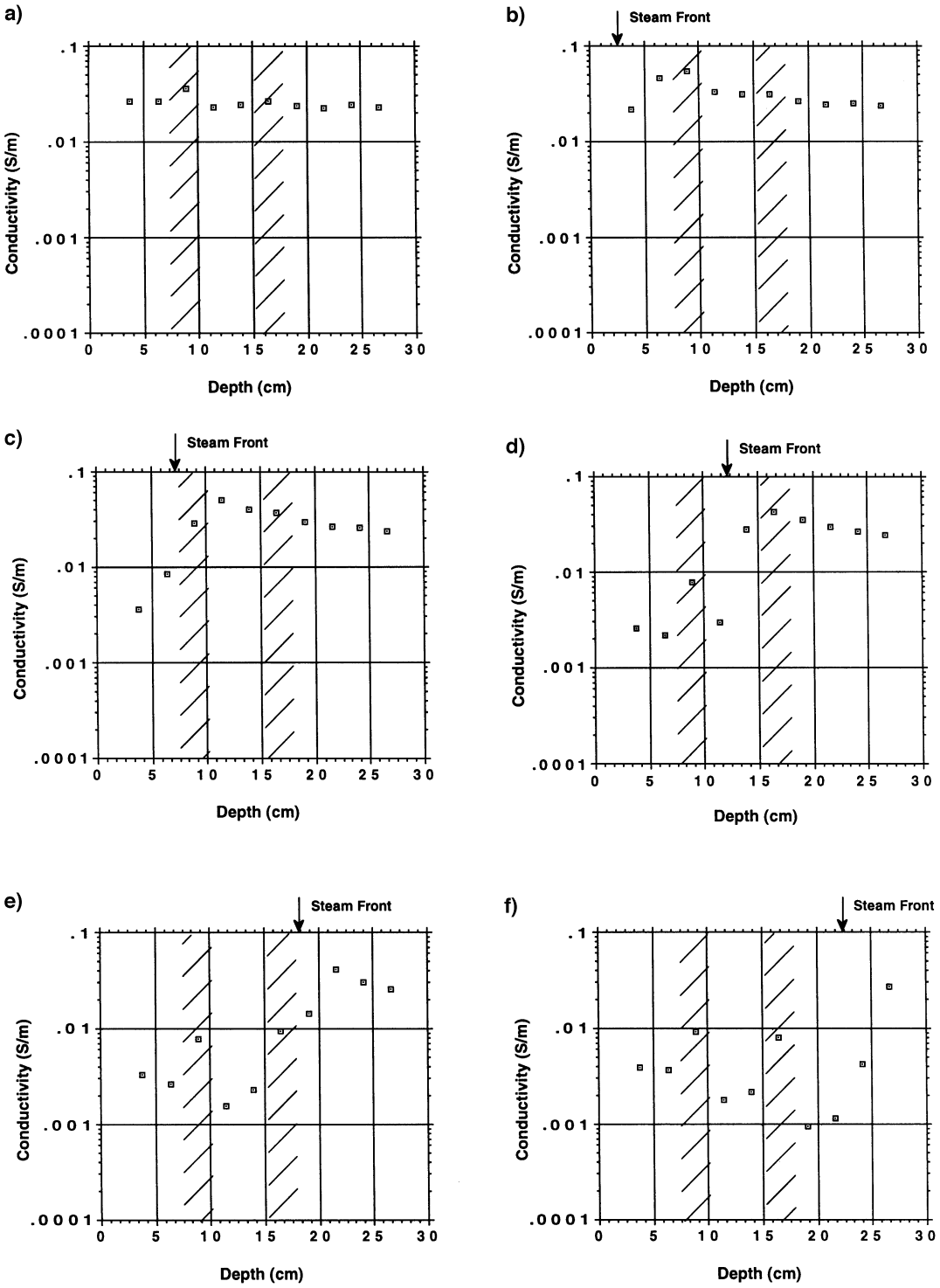

FIG. 5. Conductivity as a function of depth in the cell at six times in the experiment: (a) 0 s, (b) 3600 s, (c) 4300 s, (d) 5000 s, (e) 5700 s, and (f) 6400 s. Hatched zones correspond to clay lens (7–10 cm) and sand-clay layer (15–18 cm).

Figure 5a corresponds to the starting condition. The initial conductivities are nearly equivalent at approximately 0.025 S/m, except for the third datum from the left, σ_3, which is slightly more conductive and represents the upper clay lens. The remaining five slices correspond to the arrival of steam at the first, third, fifth, seventh, and ninth thermocouples. In Figure 5b the steam front is at the first thermocouple, at the top of σ_1's measurement region. Conductivity σ_1 has begun to decrease, while σ_2 and σ_3, at the next two locations, have increased. Deeper than 10 cm into the sand, the conductivities remain close to their original values. In Figure 5c the steam front has reached the top of the clay lens. Conductivities in the steam zone (those data to the left of the arrow) have decreased considerably. Conductivity ahead of the steam front (to the right of the arrow) increases with depth, reaching a maximum 4.5 cm ahead of the front. In Figure 5d the steam front has reached thermocouple T_5. In the steam zone, the anomalously high conductivity of the clay lens (σ_3, third datum from the left) is apparent and is situated between two more resistive sand regions. Ahead of the steam front, a similar profile exists as in Figure 5c, with conductivity reaching a maximum 4.5 cm ahead of the front, then decreasing farther into the sand. This panel shows the first indication of a conductivity minimum forming in the steam zone at a depth of 6.5 cm and a magnitude of 0.002 S/m. The last two slices show that this minimum moves with the steam front and decreases in magnitude over time. In Figure 5e the minimum is 0.0015 S/m at 11.5 cm, and in Figure 5f it is 0.00095 S/m at 19 cm. Thus, the steam front is always located downstream of the conductivity minimum and upstream of the conductivity maximum. The last slice also clearly shows that the two clay regions, at 8.5 and 16.5 cm, have conductivities in the steam zone that are much higher than in the surrounding sands.

The average residual water saturation in the steam zone, S_{wres}, was determined to be 0.14 ± 0.07. This was estimated by measuring the volumetric difference between the total outflow from the cell and the total inflow into the boiler when steam broke through the end of the cell. The initial water saturation in the cell before the experiment was assumed to be 100%. The volumetric difference, as a fraction of the total pore volume of the cell, gives the average steam saturation S_{steam}, and $S_{\text{wres}} = 1.0 - S_{\text{steam}}$.

NUMERICAL MODELING

The steam-flooded clay regions in this experiment were more conductive than the surrounding steam-flooded clean sands. We wished to determine whether this increased conductivity in the clay was caused primarily by clay conduction or whether it was a result of a higher steam-zone water saturation in the clay than in the sand. To do this, we used the numerical steam-flood model of Butler and Knight (1995). It calculates the temperature, salinity, and saturation profiles that would result from the injection of steam into a 1-D clean sand. It then uses equation (1) to calculate the electrical conductivity profile. By numerically reproducing the measured conductivity responses in the clean sand, we are able to separate, in the clay regions, the effects of clay conductivity and increased water saturation.

The model requires a number of input parameters. Among these are the porosity and cross-sectional area of the sand, the original pore-fluid salinity and the boiler feed-water salinity, the pump rate into the boiler, the steam quality, and the speed of the steam front. All of these are known before the experiment, except for the front speed, which is measured directly. The model also requires estimates of the thermal conductivity and the ionic dispersivity of the sand. An important final input parameter is an estimate of the residual water saturation in the steam zone, in the clean sand. This, along with the steam-liquid salinity and the steam-zone temperature, determines the equilibrium conductivity at late time in the steam zone. By numerically reproducing the measured temperature and conductivity data from the clean-sand regions, we inferred salinity and saturation distributions in the clean sand. The clay-bearing regions in this experiment—in particular, the sand-clay layer—experienced temperature and salinity variations nearly identical to those in the clean sand. We therefore used the same calculated temperature, salinity, and water saturation distributions to predict the conductivity responses of the clay regions, using equations (2), (3), and (4). These equations accounted for clay conductivity but not for any increased water saturation in the clay. If the predicted responses in the clay match the measured data, then the increased conductivity in the clay steam zones resulted only from clay surface conduction. If not, then it also resulted from increased water saturation.

Measured and modeled temperature data are shown in Figure 6. In the experiment, a preheating interval of 3130 s is required for the top steel plate to be heated to steam temperature before steam can move through the sand. The model does not simulate the preheating. Instead, it produces a temperature distribution (closer to a step function) that would occur if no steel plate existed. Modeled data are therefore delayed by 3130 s. Temperatures from the deeper regions in the cell are better matched as the effect of the steel plate decreases with distance. As well, the model assumes a constant steam-front speed, whereas the actual speed varies in the experiment.

Measured and modeled conductivities in the clean sand (σ_1, σ_2, σ_4, σ_7, σ_8, σ_9, and σ_{10}) are compared in Figure 7. Trace σ_5 was not included because it seemed affected by clay. Modeled conductivities match well the initial increases prior to the steam front's arrival, the decreases coinciding with the passage of the steam front, and the final value in the steam zone. The residual water saturation in the steam zone (an input parameter) is adjusted to obtain a good match between the predicted and measured final conductivities in the steam zone. The inferred saturation was 0.12. This is within the measured range of 0.14 ± 0.07.

Some disagreements exist between measured and modeled data. First, the initial increase in measured conductivity, before

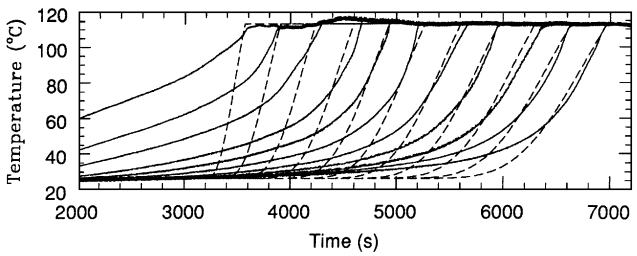

FIG. 6. A comparison of measured (solid) and calculated (dashed) temperatures for the steam-flood experiment. Temperatures are shown as functions of time for the 11 thermo-couples in the cell.

the arrival of the steam front, occurs long before the modeled increase does. This is caused by the model's inability to account for a preheating stage (see Figure 6). Second, the large drop in conductivity occurs earlier and less rapidly in the measured data than in the modeled response. We suggest this is attributable to a small amount of air in the sand, probably caused by imperfect evacuation of the cell prior to initial saturation. Air is stable at temperatures and pressures that would cause steam vapor to condense. Therefore, an air phase can develop ahead of the steam front, reducing the saturation at a given position before the steam front arrives. The model assumes a fully water-saturated region ahead of the steam front. Third, the width of the modeled conductivity minimum is narrower than the measured one. None of these failings of the model will affect its ability to correctly predict the equilibrium conductivity in the steam zone.

The predicted salinity, saturation, and temperature distributions may now be used to predict the conductivity in the clay. The sand-clay layer between thermocouples T_6 and T_7 is ideally suited for comparison. Since it was subjected to the same steamflood conditions as the clean sands, it experienced the same temperature and salinity variations. The clay lens between thermocouples T_3 and T_4 will be neglected in this analysis; it was initially packed dry and became heavily fractured upon saturation. In addition, the flow between T_3 and T_4 was likely not 1-D. Below T_4, however, the flow would have quickly become 1-D again as a result of the self-stabilizing nature of the downward-traveling steam front.

Using a clay cation exchange capacity of 0.033 meq/g (obtained from the Source Clay Minerals Repository at the University of Missouri-Columbia where the clay was obtained) and the porosity and density of the sand-clay layer, a value for Q_v of 0.01 meq/cm^3 was calculated. Equations (2), (3), and (4) are then used to calculate the conductivity in the clay layer. The measured and modeled data for both the sand and clay regions are shown as time slices in Figure 8. Clay regions are shown by the two hatched areas. The position of the steam front is marked in each time slice by a vertical arrow. The modeled conductivities match the measured conductivities ahead of the steam front, except for the discrepancy immediately ahead of the front that, as noted earlier, is likely a result of an air phase forming ahead of the front.

The measured conductivities in the sand regions are well matched in the steam zone by the modeled values, particularly in the later time slices. The measured conductivity in the lower clay region, however, is much higher than the predicted value. The steam-zone residual saturation used in the model calculations was 0.12, the value determined for the clean-sand regions. To match the measured steam-zone conductivity for the clay, a water saturation of 0.18 is required. This saturation is within the measured limits of the average saturation over the entire steam zone. Thus, the clay in this region has effectively increased the steam-zone water saturation. Furthermore, the increased saturation helps to explain the decreased steam-front speed in the clay regions because front speed and water saturation are inversely related (Stewart and Udell, 1988). The closer agreement between the measured and modeled data from the upper clay lens (between 0.075 and 0.105 m) is misleading and should be ignored for two reasons. First, the modeled data assume a 1-D layer in this region, where in fact the layer was a clay lens surrounded by clean sand. Second, the lens became heavily fractured during the experiment. Thus, it is difficult to represent the region as a homogeneous layer.

Clay content in the deeper layer was small, resulting in a clay conduction term which was small in comparison to the bulk conduction term. The dominant factor responsible for the steam zone being more conductive in the clay than in the clean sand was the increased residual water saturation in the clay. To extend the results to consider higher levels of clay, we used the numerical model. The experimental cell, with a temperature limit of 140°C, could not operate at the higher steam-zone pressures and temperatures that would result from higher clay content. Therefore, the model will be used to predict conductivity responses in reservoirs with clay contents outside the model's tested region.

By calculating theoretical conductivity responses of different reservoirs, one can determine under various circumstances

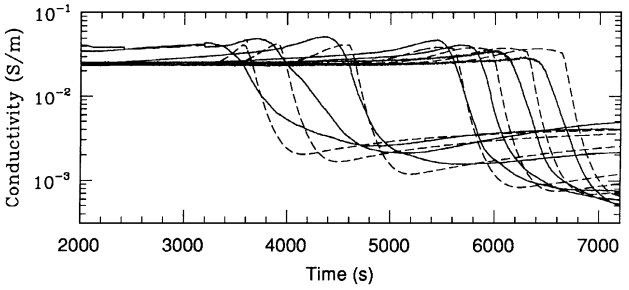

FIG. 7. A comparison of measured (solid) and calculated (dashed) conductivities in the clean sand region of the cell. Conductivities are shown as functions of time for the measurement locations of Figure 3.

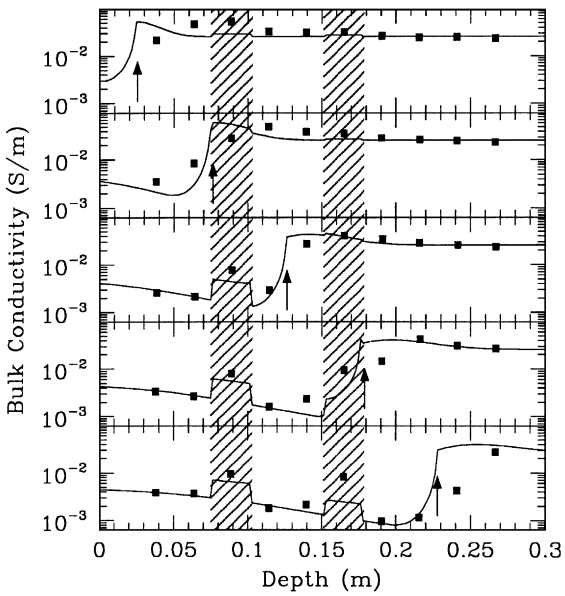

FIG. 8. A comparison of measured conductivities (squares) and corresponding model results (solid lines), showing values as functions of position, at different times. Hatched regions correspond to clay regions in the cell. Arrows in each profile mark the position of the steam front.

whether a steam zone will be conductive or resistive relative to initial conditions. Two examples of clay-bearing materials are shown here. Both are commercial hydrocarbon-bearing reservoir rocks: Noxie Sandstone and Torpedo Sandstone.

Porosity ϕ, clay content C_c, cation concentration Q_v, and hydraulic permeability k for these rocks are given in Table 1. Cation concentration is a function of porosity, clay content, and the cation exchange capacity of the clay, which can vary between clay minerals and between individual specimens of one clay mineral. In this example, while porosities and clay contents of the two sandstones are similar, the cation concentrations are 0.07 and 0.25 meq/cm^3. These are significantly higher than the 0.01 meq/cm^3 in the laboratory experiment.

Permeability depends in part on the amount of clay present in a sandstone and the geometric distribution of the clay relative to the pore throats. For this example, permeability is higher for pore-lining clays that do not obstruct pore throats, as in the Noxie Sandstone, and is lower for pore-bridging clays that close off pore throats, as in the Torpedo Sandstone. Irreducible water saturations were calculated from the porosities and permeabilities using equation (5).

The numerical model was used to determine the electrical response of these rocks under particular injection conditions. Using a high steam quality of 75%, which is typical of most field scenarios, the examples were subjected to three different steam floods using initial pore-fluid salinities of 0.01, 0.1, and 1.0 mol/liter NaCl. This covers the typical range of oil-reservoir salinities. Boiler feed-water and original pore-fluid salinities were kept equal to simulate field conditions. The injection rate into the boiler was identical for all simulations. The porosities and irreducible water saturations in the two rocks result in equivalent steam-front velocities v_f of 2.6×10^{-5} m/s. These speeds were calculated by balancing heat flows across the steam fronts (Menegus and Udell, 1985).

Simulation results are given in Figure 9. Each panel shows conductivity, normalized to the starting conductivity, as a function of distance at five times. The vertical dashed line in each panel shows the location of the steam front. Panels are arranged so that cation concentration increases to the right and salinity increases downward. Figures 9a and 9b display results of the 0.01 M NaCl calculations for Noxie Sandstone ($Q_v = 0.07$ meq/cm^3) and Torpedo Sandstone ($Q_v = 0.25$ meq/cm^3), respectively. Figure 9a shows that the section of the steam zone close to the front, immediately to the left of the dashed line, is resistive (conductivity ratio <1). In fact, this is the most resistive portion in the reservoir. As the steam flood progresses through time slices t_1 to t_5, this minimum in conductivity moves with the front. As well, the minimum deepens between times t_1, t_2, and t_3. At t_4, the minimum reaches a stable value, and by t_5 it begins to broaden. The equilibrium steam-zone conductivity, shown at the left of each time slice, is slightly higher than the initial conductivity. In Figure 9b, which represents Torpedo Sandstone, the section of the steam zone close to the front is again the least conductive part of the reservoir. However, its conductivity is nearly identical to the initial conductivity. As well, it reaches a stable minimum conductivity and begins to broaden at t_2, instead of t_4 in the case of Figure 9a. The equilibrium steam-zone conductivity in Figure 9b is significantly higher than the initial conductivity. The major differences in results between the two simulations are that as Q_v increases and permeability decreases, clay conduction and steam-zone water saturation increase.

Figures 9c and 9d use the same two reservoirs, but the simulations are for 0.1 M NaCl. Figure 9c shows three significant differences from Figure 9a. First, the equilibrium steam-zone conductivity ratio in Figure 9c is slightly less than one. Second, the portion of the steam zone close to the front is substantially more resistive in Figure 9c and does not reach a stable conductivity until t_5. Third, the conductivity ratio immediately ahead of the steam front in Figure 9c is also less than one. These differences reflect the increased salinity contrast between the original pore fluid and distilled water, which condenses at the steam front and drastically lowers the surrounding conductivity. It also indicates that the magnitude of the bulk conduction term, relative to the clay conduction term, is greater in this simulation than in Figure 9a. The clay-induced increases in relative steam-zone conductivity that occur between Figures 9a and 9b are also evident between Figures 9c and 9d. In Figure 9d, the steam zone is eventually more conductive than the initial conditions, but a substantially resistive portion still appears near the steam front.

The bottom two panels illustrate the 1.0-M NaCl simulations. They further illustrate how increasing salinity increases the relative importance of the bulk conduction term, thereby accentuating the development of a steam-zone conductivity minimum close to the steam front. As well, increasing the salinity further reduces the relative conductivity of the steam zone, so the equilibrium conductivity ratios in Figures 9e and 9f are less than those in Figures 9c and 9d.

Half of these simulations produce steam zones that are conductive relative to initial conditions. However, all but one show at least part of the zone to be more resistive than initial

Table 1. Reservoir parameters used in numerical investigation of the relationship between clay content and steam-flood conductivity response.

	Porosity	Clay content	Q_v (meq/cm^3)	Permeability (m^2)	Irreducible water saturation
Noxie Sandstone	0.27	5% kaolinite, 1% chlorite, 7% illite, as pore lining clays	0.07	4.2×10^{-13}	0.26
Torpedo Sandstone	0.245	6% kaolinite, 7% illite, as pore-bridging clays	0.25	9.4×10^{-14}	0.40

Data taken from Lake (1989).

conditions. The resistive sections grow with time, reflecting the growth of distilled water banks at the steam fronts that dilute pore-fluid salinities. Thus, regardless of clay content, a conductivity minimum almost always appears at the front of the steam zone.

The final factor that must be considered is the steam-flood fluid response. If the steam front moves more quickly than the injected steam liquid, then salt dilution at the front becomes a dominant factor, strongly reducing the conductivity as in the examples above. In the field, steam fronts typically advance very slowly as a result of heat losses to the surrounding rocks. Stewart and Udell (1988) also show that if a significant oil saturation exists before steam flooding, the front slows its advance as an oil bank forms ahead of it. For water-saturated materials, a slow steam front can be produced in the absence of heat losses by using low-quality steam. Therefore, numerical simulations for Noxie and Torpedo Sandstones were repeated using a steam quality of 25%. This results in a steam front speed of 1.1×10^{-5} m/s.

Corresponding conductivity profiles are displayed in Figure 10. (The times t_1 through t_5 are different than those in Figure 9. We wished to show the steam front in the same locations

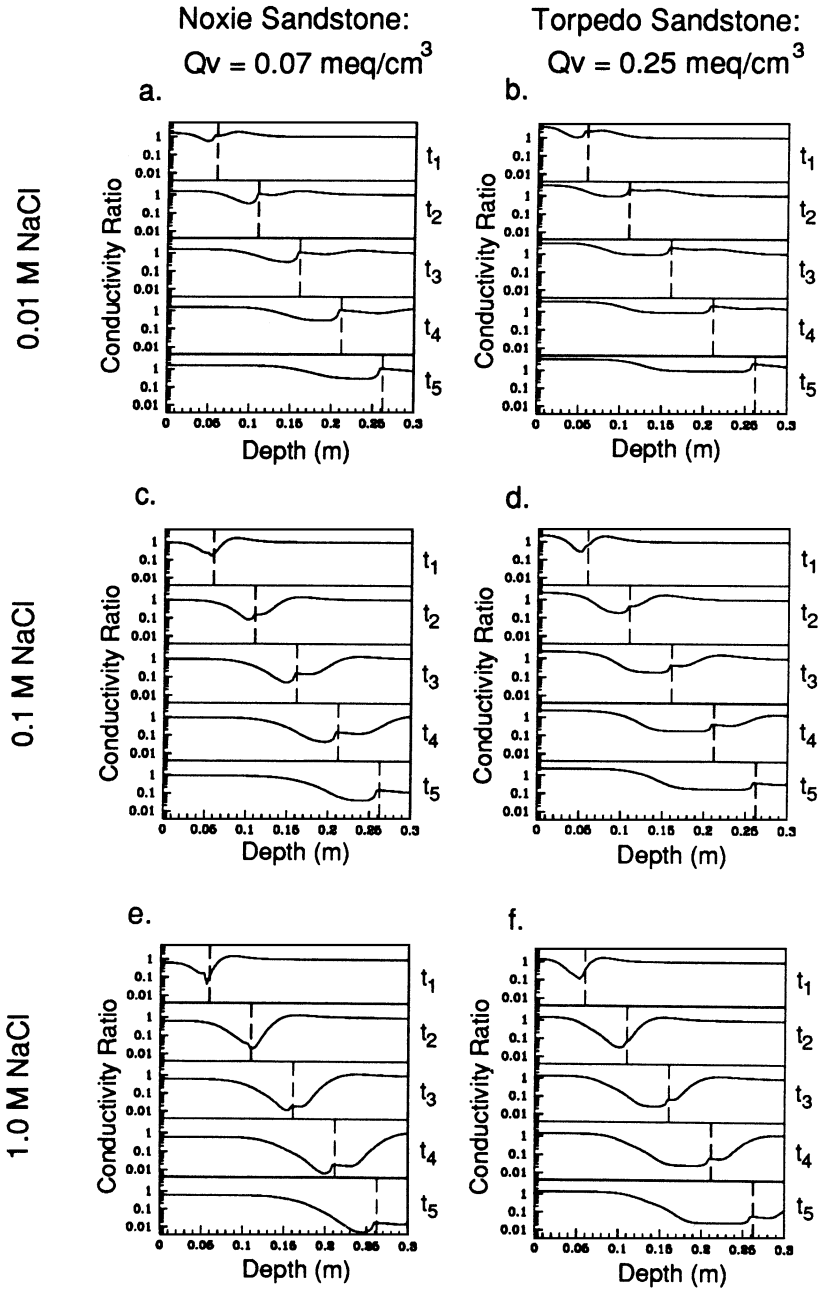

FIG. 9. Simulations of conductivity versus time and depth in the cell for a fast steam front. Steam quality is 75%, and steam-front speed is 2.6×10^{-5} m/s. Clay cation concentration increases to the right, and salinity increases downward. Data are plotted as the logarithm of the ratio of conductivity to initial conductivity. Dashed lines mark the positions of the steam fronts.

as in Figure 9; therefore, we chose later times because the speed of the steam front is reduced in this case.) All simulations produce profiles that are flat throughout most of the steam zone, increase slightly at the steam front because of increasing water saturation, and fall ahead of the steam front because of decreasing temperature. In Figures 10b and 10d, the steam zones are entirely conductive. These results show the importance of the steam-flood fluid response. When the steam front moves slowly, the steam zone shows a nearly uniform conductivity, with a conductivity high at the front. Since a distilled water bank is unable to form at the front, salinity ceases to be a factor governing conductivity, which then responds only to saturation and temperature variations.

SUMMARY AND CONCLUSIONS

Clay increases the electrical conductivity of steam zones through two mechanisms. First, it provides a conduction path

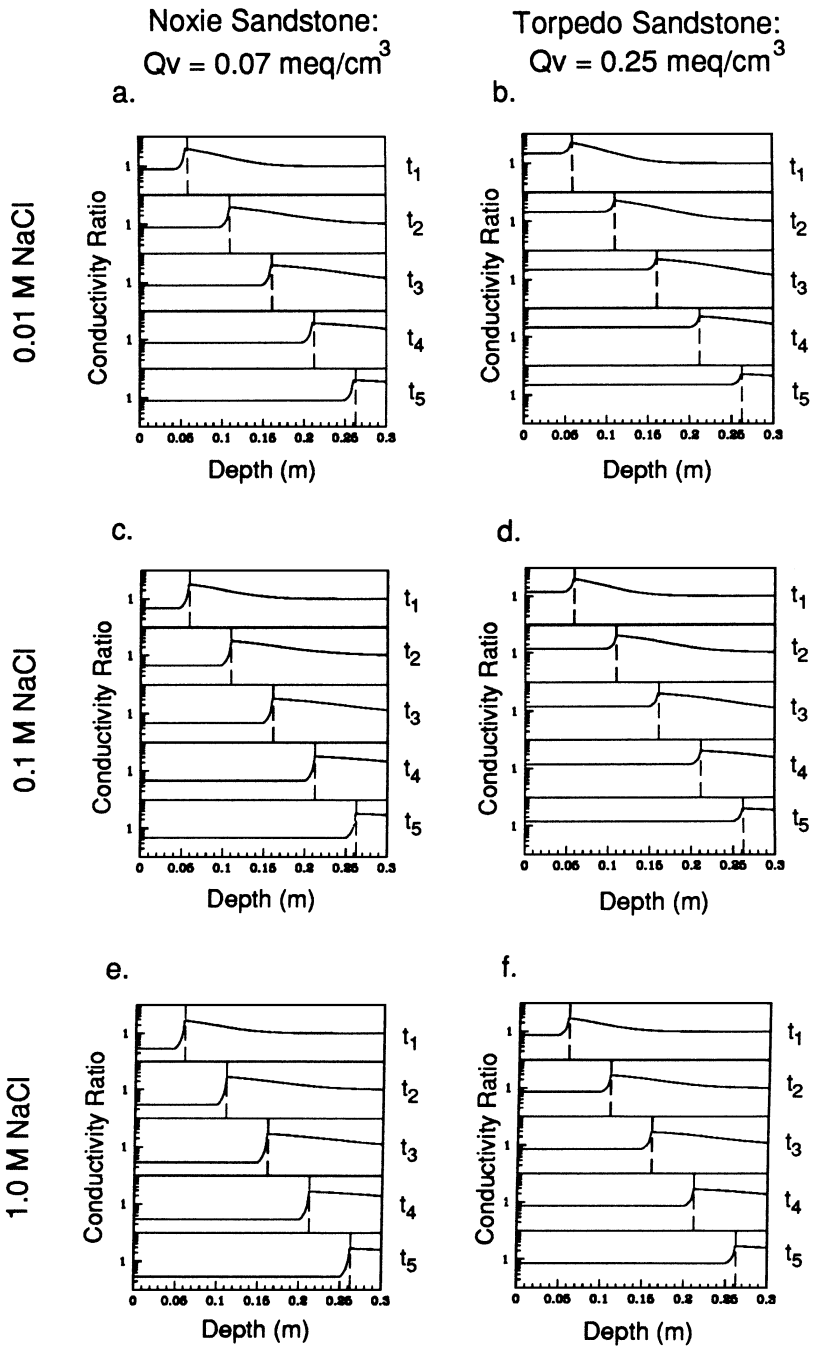

FIG. 10. Simulations of conductivity versus time and depth in the cell for a slow steam front. Steam quality is 25%, and steam-front speed is 1.1×10^{-5} m/s. Clay cation concentration increases to the right, and salinity increases downward. Data are plotted as the logarithm of the ratio of conductivity to initial conductivity. Dashed lines mark the positions of the steam fronts.

along its surface that is more sensitive to temperature changes and less sensitive to saturation changes than is conduction through the bulk pore fluid. Second, the presence of clay results in higher steam-zone residual water saturations. This results in steam-flooded material with a high clay content eventually becoming conductive relative to initial conditions, particularly if original pore water and boiler feed water are fresh. Whether the entire steam zone becomes conductive depends on the speed of the steam front relative to the injected steam liquid, which carries the dissolved salts from the boiler feed water. If the steam front is relatively fast, the additional conductivity from the clay is insufficient to make the region close to the steam front conductive because this region is dominated by a distilled water bank. If the front is relatively slow, then a distilled water bank does not form and the entire steam zone can become conductive.

In the experimental results, a distilled water bank led to large decreases in conductivity in a narrow region close to the steam front. This region was approximately 20 cm long. The width of this region is a function of the size of the measurement apparatus. In a field scenario, its width will grow with time in proportion to the differences in speed between the steam front and the steam liquid. Therefore, at field scales of tens to hundreds of meters, the low-conductivity region should be large enough to be easily detectable by techniques such as electrical resistance tomography.

There are clearly numerous complex physical and chemical processes associated with the movement of steam through a saturated porous material. Some of these processes result in changes in the system that lead to detectable, and predictable, changes in the electrical properties of the material. In this study we have attempted to systematically identify and assess the role of a number of factors that contribute to the electrical response observed during a steam flood. We find that the electrical conductivity of a steam-flooded material, at any given time, is largely determined by the temperature, the salinity of the water, the water saturation, and contributions from clay surface conduction, with these last two factors being a function of the lithology and pore structure of the material. We find that the specific nature of the time-dependent changes in conductivity, while affected by the hydraulic properties of the material, is also strongly governed by the fluid response of the steam flood. The relative speeds of the steam liquid and steam gas phases, determined in part by the steam quality, are key factors in determining the temporal variation in conductivity throughout the flood. By recognizing and studying both these material-dependent and fluid-response-dependent factors, we have provided a laboratory and numerical basis for the interpretation, and prediction, of the electrical response of steam-flooded geological materials.

ACKNOWLEDGMENTS

The development and construction of the laboratory steamflood apparatus was funded by Mobil Exploration and Production Services and Mobil Research and Development. We are grateful to Bill Troyer for initially suggesting this project and to Jim Bulau and Ranga Ranganayaki for helpful discussions during the early stages of this research. Additional funding was obtained through an NSERC operating grant to R. Knight. David Butler was supported by an NSERC scholarship and by a Tri-Council Eco-Research scholarship. We also thank Michael Wilt for very helpful comments and discussions.

REFERENCES

Archie, G. E., 1942, The electrical resistivity log as an aid in determining some reservoir characteristics: AIME, **146**, 54–67.

Butler, D. B., and Knight, R. J., 1995, The effect of steam quality on the electrical conductivity of steamflooded sands: A laboratory study: Geophysics, **60**, 998–1006.

Clavier, C., Coates, G., and Dumanoir, J., 1984, Theoretical and experimental bases for the dual-water model for interpretation of shaly sands: Soc. Petr. Eng. J., **24**, 153–167.

Donaldson, E. C., Chilingarian, G. V., and Yen, T. F., Eds., 1985, Enhanced oil recovery **II**: Processes and operations: Elsevier Science Publ. Co., Inc.

Hill, H. J., and Milburn, J. D., 1956, Effect of clay and water salinity on electrochemical behavior of reservoir rocks: Trans. Am. Inst. Min., Metall., **207**, 65–72.

Lake, L. W., 1989, Enhanced oil recovery: Prentice-Hall, Inc.

Mansure, A. J., Meldau, R. F., and Weyland, H. V., 1990, Field examples of electrical resistivity changes during steamflooding: 65th Ann. Tech. Conf. and Exhib., Soc. Petr. Eng., Expanded Abstracts, 109–119.

Menegus, D. K., and Udell, K. S., 1985, A study of steam injection into water saturated capillary porous media, *in* Yao, L. S., Chen, M. M., Hickox, C. E., Simpkins, P. G., Chow, L. C., Kaviany, M., Cheng, P., and Davis, L. R., Eds., Heat transfer in porous media and particulate flows: **46**, Am. Soc. Mech. Eng., 151–157.

Newmark, R. L., and Wilt, M. J., 1992, Changes in formation electrical properties during steam floods: 62nd Ann. Internat. Mtg., Soc. Expl. Geophys., Expanded Abstracts, 488–491.

Patnode, H. W., and Wyllie, M. R. J., 1950, The presence of conductive solids in reservoir rocks as a factor in electric log interpretation: Trans. Am. Inst. Min., Metall., **189**, 47–52.

Ramirez, A., Daily, W., LaBrecque, D., Owen, E., and Chestnut, D., 1993, Monitoring an underground steam injection process using electrical resistance tomography: Water Resour. Res., **29**, 73–88.

Ranganayaki, R. P., Akturk, S. E., and Fryer, S. M., 1992, Formation resistivity variation due to steam flooding: A log study: Geophysics, **57**, 488–494.

Sen, P. N., and Goode, P. A., 1992, Influence of temperature on electrical conductivity of shaly sands: Geophysics, **57**, 89–96.

Stewart, L. D., and Udell, K. S., 1988, Mechanisms of residual oil displacement by steam injection: Soc. Petr. Eng. Reservoir Eng., **3**, 1233–1242.

Timur, A., 1968, An investigation of permeability, porosity, and residual water saturation relationships for sandstone reservoirs: The Log Analyst, 8–17.

Vaughan, P. J., Udell, K. S., and Wilt, M. J., 1993, The effects of steam injection on the electrical conductivity of an unconsolidated sand saturated with a salt solution: J. Geophys. Res., **98**, No. Bl, 509–518.

Waxman, M. H., and Smits, L. J. M., 1968, Electrical conductivities in oil-bearing shaly sands: Soc. Petr. Eng. J., **8**, 107–122.

Waxman, M. H., and Thomas, E. C., 1974, Electrical conductivities in shaly sands–**I**. The relation between hydrocarbon saturation and resistivity index; **II**. The temperature coefficient of electrical conductivity: J. Petr. Tech., **26**, 213–225.

Winsauer, W. O., and McCardell, W. M., 1953, Ionic double-layer conductivity in reservoir rocks: Trans. Am. Inst. Min., Metall., **198**, 129–134.